ATMOSPHERIC CORRECTIONS OF LAND IMAGERY USING THE EXTENDED RADIOSITY METHOD

Christoph C. Borel and Siegfried A.W. Gerstl
Space Science & Technology Division
Los Alamos National Laboratory, MS D-438
Los Alamos, New Mexico 87545, USA

Abstract

In this paper we describe an application of the extended radiosity method to compute atmospheric scattering effects over heterogeneous surfaces and to perform the inverse operation: to correct for such atmospheric effects. The radiosity method is used to compute point-spread-functions (PSF's) which determine how much light is scattered from an adjacent surface into the field-of-view (FOV) of a sensor above the atmosphere. We show that the PSF's are in general asymmetric for pointable airborne or satellite sensors. A Fourier transform based method can be used to correct adjacency-effect-blurred images for these atmospheric distortions.

1 Introduction

When images of heterogeneous land surfaces are acquired through the atmosphere, the measured radiance data include not only the surface radiances per pixel but also contain modifications due to the atmosphere. Correcting such modified land imagery for atmospheric effects, one must consider atmospheric absorption as well as scattering. In this paper we concentrate on the atmospheric scattering that gives rise to a blurring effect of adjacent pixels. The adjacency-blurring-effect is most noticeably observed at the boundary between a dark and a bright surface. Near the edge over a dark surface photons from the nearby bright surface may be scattered within the atmosphere into the field of view (FOV) of an airborne or satellite sensor. Conversely, near the edge over a bright surface fewer photons reach the sensor's FOV. At a discontinuity in the surface reflectance, the intensity transect in a satellite image appears therefore as a sigmaoid instead of a step function. This blurring effect is most often observed at boundaries between surfaces with a large contrast ratio such as water and land in the visible, and has been described in the literature by Diner (1985), Kaufman (1984), Richter (1990), Pearce (1977), Tanré (1980) and others.

The adjacency-blurring-effect may introduce errors in the classification of small bright areas surrounded by a dark region, or dark areas on a bright background (Kaufman (1984)). One can model the blurring due to the adjacency effect with a point spread function (PSF). That PSF is a filter function which is convolved with the unperturbed (no atmosphere) image of a surface. Most PSF's are generated by Monte Carlo-based methods and are assumed to be rotationally symmetric and thus, are not valid for off-nadir views. In the situation of a pointable sensor, it is necessary to compute off-nadir PSF's which are generally asymmetric.

We introduce a simple method to compute the asymmetric point spread function for any view direction and any layered atmosphere. The method is based on the extended radiosity method (Borel and Gerstl (1991)) also sometimes called zonal method (Hottel (1967)). Computational methods will be discussed as well as the rendering of various scenes using computer graphics methods.

Using the inverse filter of the PSF it is possible to correct the adjacency-blurred image and restore the unperturbed contrast ratios at reflectance discontinuities.

2 Summary of the Volume Radiosity Method

In this paper we discuss on a method based on the principles of volume or extended radiosity (Rushmeier (1989), Borel and Gerstl (1991)). The extended radiosity method is based on radiative transfer and considers energy exchange between volume/volume, volume/surface, surface/volume and surface/ surface elements. It assumes :

1. Isotropic, volumetric emission and scattering by the participating medium for the volume elements
2. Diffuse (Lambertian) reflection from opaque surfaces
3. Arbitrary directional illumination

The volume radiosity was developed by heat transfer specialists (e.g. Hottel (1967)) and is also known as the zonal method in the literature. The set of simultaneous linear algebraic equations for the radiosity method are given by (Hottel (1967)) :

$$B_i^s\ A_i \quad = \quad E_i^s\ A_i\ +\ \rho_i \left[\sum_{j=1}^{N_s} B_j^s\ F_{ji}^{ss}\ + \right.$$
$$\left. +\ \sum_{k=1}^{N_v} B_k^v\ F_{ki}^{vs} \right] \ , \quad i\ =\ 1, \ldots, N_s, \qquad (1)$$

$$4\ \kappa_{t,k}\ B_k^v\ V_k \quad = \quad 4\ \kappa_{a,k}\ E_k^v\ V_k\ +\ \alpha_k \left[\sum_{j=1}^{N_s} B_j^s\ F_{jk}^{sv}\ + \right.$$
$$\left. +\ \sum_{m=1}^{N_v} B_m^v\ F_{mk}^{vv} \right] \ , \quad k\ =\ 1, \ldots, N_v, \ (2)$$

where B_i^s is the surface radiosity in $[W\ m^{-2}]$, E_i^s is the emission in $[W\ m^{-2}]$ and ρ_i is the reflectance $[unitless]$ of surface patch i

with area A_i. The flux density in $[W]$ leaving a volume element k is given by $4\ \kappa_{t,k}\ B_k^v\ V_k$ where $\kappa_{t,k}$ is in $[m^{-1}]$ and is the sum of the absorption coefficient $\kappa_{a,k}$ and the scattering coefficient $\kappa_{s,k}$, and B_k^v in $[W\ m^{-2}]$ is the volume radiosity. The scattering albedo of the k-th volume element is $\alpha_k\ =\ \kappa_{s,k}/\kappa_{t,k}$. Eqs. (1) and (2) state that the volume and surface radiosities are given by the sums of the emission and the scattered and reflected radiosities from all other surfaces and volumes. The view factors are defined as the ratio of the total energy emitted or scattered by a surface or volume arriving at another surface or volume divided by the radiosity of the source surface or volume. The view factors from a surface k to surface j is F_{kj}^{ss} in $[m^2]$, the view factor from volume k to surface i is F_{ki}^{vs} in $[m^2]$, the view factor from surface j to volume k is F_{jk}^{sv} in $[m^2]$, the view factor from volume m to volume k is F_{mk}^{vv} in $[m^2]$. The view factors depend on the geometry and attenuation of fluxes between elements and are usually difficult to evaluate in general (Hottel (1967)) and simple approximations for certain geometries exist (Borel and Gerstl (1991)).

Eqs. (1) and (2) assume that the surfaces are Lambertian reflectors so that the light is scattered equally in all directions. Three dimensional structures like clouds, fog and smoke may be simulated by assigning absorption and scattering characteristics independently for each volume element V_k.

The intensity I of the light in $[W\ m^{-2}]$ reaching the observer from a certain direction or along a ray is given by (Rushmeier (1987)):

$$I(L)\ =\ \exp(-\kappa_t\ L)\ \frac{B_i^s}{\pi}\ +\ \int_0^L\ \exp(-\kappa_t\ l)\ \frac{B^v(l)}{\pi}\ \kappa_t\ dl, \quad (3)$$

where $I(L)$ is the radiative intensity on the outside of the scattering medium, L is the distance between the entrance point of a ray to the exit point. If the exit point lies on the surface the attenuated radiosity B_i^s must be added to the integral. The volume radiosity $B^v(l)$ along a ray from 0 to L can be found by trilinear interpolation in x, y and z of the volume radiosities which are obtained by solving the eqs. (1) and (2) with the Gauss-Seidel iterative method (Borel and Gerstl (1991)).

3 A Method to Compute the Measured Radiance over a Flat Surface

The adjacency effect is due to scattering of light from surrounding surfaces into the line of sight between an observed surface and sensor position. Translating this assumption into the context of the radiosity equations, one could argue that the radiosity in a volume element of a participating medium is due to volume emitted radiosity and the radiosity scattered from surrounding surfaces :

$$4\ \kappa_{t,k}\ B_k^v\ V_k \quad = \quad 4\ \kappa_{a,k}\ E_k^v\ V_k\ +\ \alpha_k \sum_{j=1}^{N_s}\ B_j^s\ F_{jk}^{sv}\ ,$$
$$k\ =\ 1, \ldots, N_v. \tag{4}$$

Next we assume that the radiosity leaving a ground surface patch is due only to reflected light from the direct energy incident from the sun E_0 attenuated by the atmosphere. The contributions from diffuse skylight are of the order of 10 to 15 % and are neglected in this derivation. The radiosity leaving the ground surface is then given by :

$$B_i^s\ A_i\ =\ E_0\ \rho_i\ \exp\left(-\frac{\kappa_t\ L}{\cos\theta_s}\right)\ A_i\ , \quad i\ =\ 1, \ldots, N_s, \tag{5}$$

where $\exp(-\kappa_t\ L/\cos\theta_s)$ is the atmospheric transmittance, θ_s is the sun zenith angle. Eq. (5) assumes no contributions from surrounding surface patches and volume elements.

The measured intensity at the sensor, located above the atmosphere at distance L and tilted by the angle θ_r from zenith is then given by eq. (3) and for a homogeneous atmosphere with K layers of equal thickness, we can approximate eq.(3) with :

$$I(L)\ =\ \exp(-\kappa_t\ L)\ \frac{B_i^s}{\pi}\ +\ \sum_{k=1}^{K}\ \exp(-\kappa_t\ (K-k)\Delta l)\ \frac{B_k^v}{\pi}\ \kappa_t\ \Delta l, \tag{6}$$

where $\Delta l\ =\ L/K\ \cos\theta_r$. Substituting eqs. (5) and (4) into eq. (6) one finds :

$$I(L)\ \ =\ \ \frac{1}{\pi}\ \left[E_0\ \rho_i\ \exp\left(-\frac{\kappa_t\ L}{\cos\theta_s}\right)\ \exp\left(-\frac{\kappa_t\ L}{\cos\theta_r}\right)\ +\ \sum_{k=1}^{K}\ \left\{\frac{\kappa_a}{\kappa_t}\ E_k^v\right.\right.$$

$$+ \frac{\alpha_k}{4\ \kappa_t\ V_k} \sum_{j=1}^{N_s} E_0\ \rho_j\ \exp\left(-\frac{\kappa_t\ L}{\cos\theta_s}\right)\ F_{jk}^{sv} \Bigg\}$$
$$\kappa_t\ \exp(-\kappa_t\ (K-k)\ \Delta l)\ \Delta l \Bigg], \qquad (7)$$

where the view factor F_{jk}^{sv} between surface patch S_j and volume element V_k is given by (Borel and Gerstl (1991)) :

$$F_{jk}^{sv} \ = \ \frac{\kappa_t\ V_k\ \tau(r_{kj})\ \cos\theta\ f(\theta_{p,k})\ A_j}{\pi\ r_{kj}^2} \qquad (8)$$

where $f(\theta_{p,k})$ is the scattering phase function, $\theta_{p,k}$ is the phase angle and $\tau(r_{kj})$ is the transmission factor $\tau(r_{kj}) = \exp(-r_{kj}\ \kappa_t)$ with the distance R_{kj} between surface element j and volume element k along the line-of-sight. The indices k refer to volume elements along a ray from the bottom of the atmosphere ($k = 1$) to the top of the atmosphere ($k = K$).

4 Computation of the Point-Spread Function

In this section we will give equations to compute the point-spread function resulting from ground to atmosphere scattering for the geometry shown in Figure 1. In an optical system the point spread function $PSF(x, y, z; x_0, y_0, z_0; \theta_r, \phi_r)$ can be defined as the scattering contribution of a surface element $dA = dx\ dy$ located at $(x, y, z = z_0)$ into the line-of-sight direction of the observer (θ_r, ϕ_r) looking at point (x_0, y_0, z_0). Using the terms for the scattering from the surface located at $(x, y, z = z_0)$ into the volumes along the line of sight (second and third line in eq. (7)) and the definition for the view factor F_{jk}^{sv} in eq. (8) the unitless PSF is given by :

$$PSF(x, y, \ldots) \quad = \quad \frac{\kappa_s\ \Delta l}{4\ \pi} \sum_{k=1}^{K} \frac{\tau(r_k)\ \cos\theta_k\ f(\theta_{p,k})\ dx\ dy}{\pi\ r_k^2}$$
$$\cdot \exp(-\kappa_t\ (K-k)\ \Delta l), \qquad (9)$$

where we set the surface radiosity:
$E_0\ \rho(x, y, z = z_0)\ \exp(-\kappa_t L_z/\cos\theta_s) = 1$
for normalization purposes and where:
$\tau(r_k) \ = \ \exp(-\kappa_t\ r_k)$,
$r_k \ = \ |\vec{P_k} - \vec{P}|$,

$$\cos\theta_k \;=\; kb_z/r_k,$$

$$\theta_{p,k} \;=\; \cos^{-1}\Big[\frac{(\vec{P}_0-\vec{P}_k)\cdot(\vec{P}-\vec{P}_k)}{|\vec{P}_0-\vec{P}_k|\;r_k}\Big]$$

The point spread function can then be computed using eq. (9) for various atmospheric scattering coefficients, scattering phase functions and view angles.

The measured scene radiance in $[W\ m^{-2}]$ at the detector location above the atmosphere is given by the sum of the attenuated direct scene radiance and the convolution of the point spread function with the weighted scene reflectance map and an additional path radiance I_{path}:

$$\begin{aligned} I_{measured}(x,y) \;=\; & \frac{E_0}{\pi}\;\exp\Big(-\frac{\kappa_t\;L_z}{\cos\theta_s}\Big)\;\Big[\rho(x_0,y_0)\exp\Big(\frac{-\kappa_t\;L_z}{\cos\theta_r}\Big) \\ & +\rho(x,y)\otimes PSF(x,y,\ldots)\Big]\;+\;I_{path}. \end{aligned} \tag{10}$$

The point spread function for $\kappa_a = 0.05/L_z,\ \kappa_t = 0.3/L_z$ and view angle $\theta_r = 45^0,\ \phi_r = 0^0$ is shown in Figure 2. The size of the scattering volume was $L_x = 900\ m,\ L_y = 900\ m,\ L_z = 900\ m$ with a volume subdivision of $N_x = 30,\ N_y = 30,\ N_z = 30$ to simulate the Landsat TM sensor spatial resolution of 30 m. The PSF is shown in a logarithmic surface plot in dB scale to emphasize the shoulders. The scattering phase function was chosen to approximate a "hazy" atmosphere using the Henyey-Greenstein phase function with the asymmetry factor $g = 0.75$ (Liou (1980)). The Henyey-Greenstein phase function is given by :

$$f(\theta_p) = \frac{1-g^2}{(1+g^2-2g\cos\theta_p)^{3/2}}. \tag{11}$$

Note that the method presented allows the computation of the point spread function for height dependent scattering and absorption coefficients and even a height dependent phase function. It is also possible to extend the method to include bidirectional reflectance distribution functions for the ground and even a three dimensional terrain. The point spread function for the later cases is then local and therefore must be computed for each pixel in the scene.

5 Removing the Adjacency Blurring Effect by Deconvolution

The convolution of the reflectance map with the point spread function may be removed by inverse filtering. A classic inverse filter method has been proposed by Kaufman (1984) for the Fourier domain :

$$I_{corrected}(x,y) \;=\; F^{-1}\Big[\frac{F[I_{measured}(x,y)]}{F[PSF(x,y,\ldots)]}\Big], \tag{12}$$

where using Kaufman's notation,

$$I_{measured}(x,y) = F^{-1}[F[I_e(x,y)]M(\omega_x,\omega_y)] + I_\beta + I_0.$$

$I_e(x,y)$ is the radiance without atmospheric effects, I_β a correction term and I_0 the upward radiance for a surface with zero reflectance. The notation $F[\cdot]$ denotes the Fourier transform, $F^{-1}[\cdot]$ the inverse Fourier transform and ω is the spatial frequency in $[cycles/m]$. The term $M(\omega_x,\omega_y)$ is the modulation transfer function (MTF) and is computed from the Fourier transform of the PSF. We implemented this method but found several problems. First, it takes a long time to compute the Fourier transformations of large images using the fast Fourier transform (FFT). Second, if the images contain additive noise, the ratio of the two Fourier transforms can get very large for high spatial frequencies and the inverse Fourier transform will create a very noisy image. This problem can be avoided if the Wiener filtering approach (Pratt (1978)) is used. Third, the point spread function must be uniform over the whole image, a condition which is not met for wide field of views where the view angles change over the image.

To correct the radiance image for the adjacency blurring effect we used the deconvolution method (Pratt (1978)). The kernel for the deconvolution or inverse point spread function is given by:

$$IPSF(x,y) = \frac{1}{N_p^4}\; F^{-1}\Big[\frac{1}{F[\rho(x_0,y_0)\exp(-\frac{\kappa_t L_z}{\cos\theta_r}) + PSF(x,y)]}\Big], \tag{13}$$

where N_p^{-4} is a factor which depends on the implementation of the FFT and N_p is the width of the PSF in pixels. We found it useful to incorporate the term $\rho(x_0,y_0)\;\exp(-\kappa_t\; L_z/\cos\theta_r)$ in the computation of IPSF, confer eq. (10). The FFT used is defined as :

$$F(\omega_x,\omega_y) \;=\; \frac{1}{N_p^2}\;\sum_{x=0}^{N_p-1}\sum_{y=0}^{N_p-1}\; f(x,y)\;\exp\Big(-\frac{j2\pi}{N_p}(x\omega_x + y\omega_y)\Big),$$

where $j = \sqrt{-1}$. We observed that for realistic atmospheric conditions the inverse PSF is a very narrow pulse and over 98 % of the integral is contained in a square of 600 m side length centered around $(x = x_0, y = y_0)$ for a sensor with 30 m resolution. In Figure 3 we show the ratio of the integral over a window of length W in $[m]$ over the integral over an area of 1800 by 1800 m for the PSF shown in Figure 2 where we expanded $L_x = 1800\ m,\ L_y = 1800\ m$. Without adjacency blurring correction the measured radiance would be smaller (92 %) over a uniform surface because of neglecting the scattering contributions from adjacent surfaces. Considering the number of necessary multiplications for a small inverse filter with a window size similar to the PSF, we found it more practical to compute the adjacency corrected reflectance image by convolving the measured radiance image with the inverse PSF, $IPSF(x, y, \ldots)$, or :

$$\rho_{corrected}(x, y) \ = \ (I_{measured}(x, y) - I_{path}) \otimes IPSF(x, y, \ldots) \ . \quad (14)$$

For an image of size $N = N_x = N_y = 512 \times 512$ and an inverse PSF of $N_p = 12 \times 12$ pixels it would take

$$M_{deconvolution} \ = \ N_x \ \times \ N_y \ \times \ (N_p)^2 = 37.7 \cdot 10^6$$

multiplications for the deconvolution method versus

$$M_{FFT} \ = \ 3 \ (N_x \ \log_2 N_x)(N_y \ \log_2 N_y) = 63.7 \cdot 10^6$$

multiplications for the FFT method. For larger images the savings are even greater. In order to save multiplications by using the deconvolution method the number of pixels N_p in the inverse filter should be less than $\sqrt{3} log_2 N$, which can be obtained by setting $M_{deconvolution} = M_{FFT}$ and solving for N_p. For example for a $N_x = N_y = 512$ image we get $N_p \leq 15$ and for a $N_x = N_y = 1024$ image we get $N_p \leq 17$ and so on. We found that the necessary filter size increases with increasing optical depth. Sensors with coarser resolution smaller filter have smaller filter sizes.

To illustrate the deconvolution method with an example we created an artificial scene containing various squares and rectangles at various sizes with constant reflectance. The PSF used the same parameters as in Figure 2 except that the total scattering cross section was increased to 0.8 and the absorption cross section to 0.032 to model a very hazy atmosphere. Figure 4 shows the adjacency blurred radiance images. The original and reconstructed reflectance image are almost identical and not shown here. The sigmaoid transitions disappear totally from the reconstructed reflectance image.

The maximum relative error between the original reflectance and the recovered reflectance was 0.1 %.

Several observations can be made. First, the radiance decreases due to the adjacency effect for small bright targets as seen for the small squares, and the thin line in the upper part of the image. Second, sharp discontinuities are smoothed out producing a sigmaoid shaped transition. Third, we noticed that the radiance of the small darker squares surrounded by the bright area is increased. Fourth, due to the asymmetry of the point spread function edges have an orientation dependent transition. For example a bright surrounded by a dark surface shows a broader transition on the near side of the observer than the transition on the far side from the observer.

We speculate that by analyzing the transitions between different size patches of ground cover one could recover the PSF and then invert for the atmospheric parameters which may then be used to deblur the image.

6 Conclusion

We have presented a method to compute the point spread function for off-nadir pointing sensors using selected parts of the radiosity equation. We showed that the point spread function is in general asymmetric. The radiosity based method is able to include scattering phase functions and atmospheric parameters for a stratified atmosphere. A Fourier transform based method is able to recover the radiance even when additive noise is present.

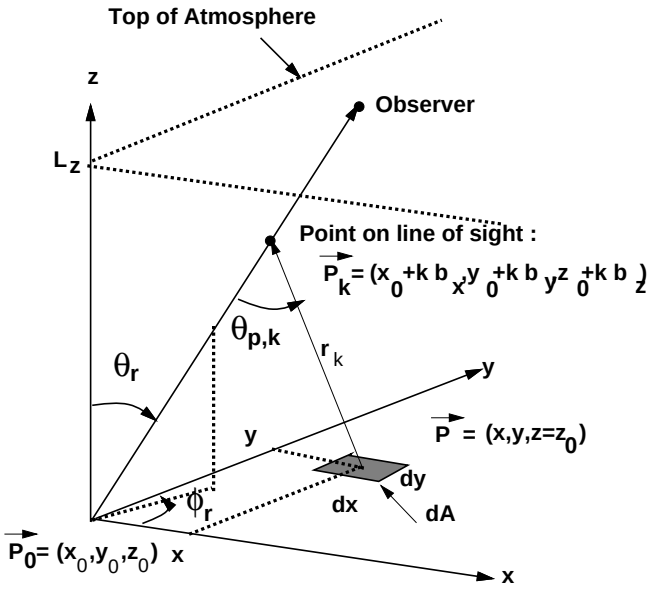

Figure 1 Geometry for computing the point spread function.

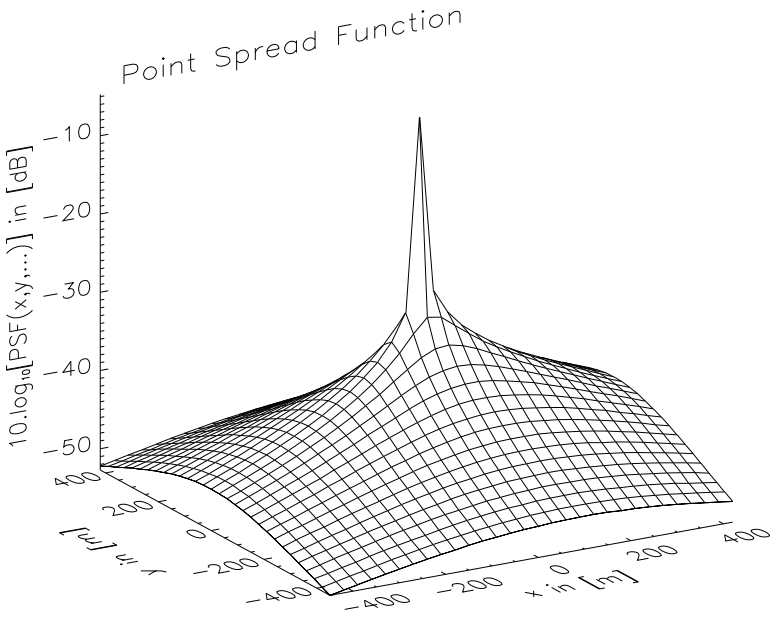

Figure 2 Point spread function for a view angle of 45^0.

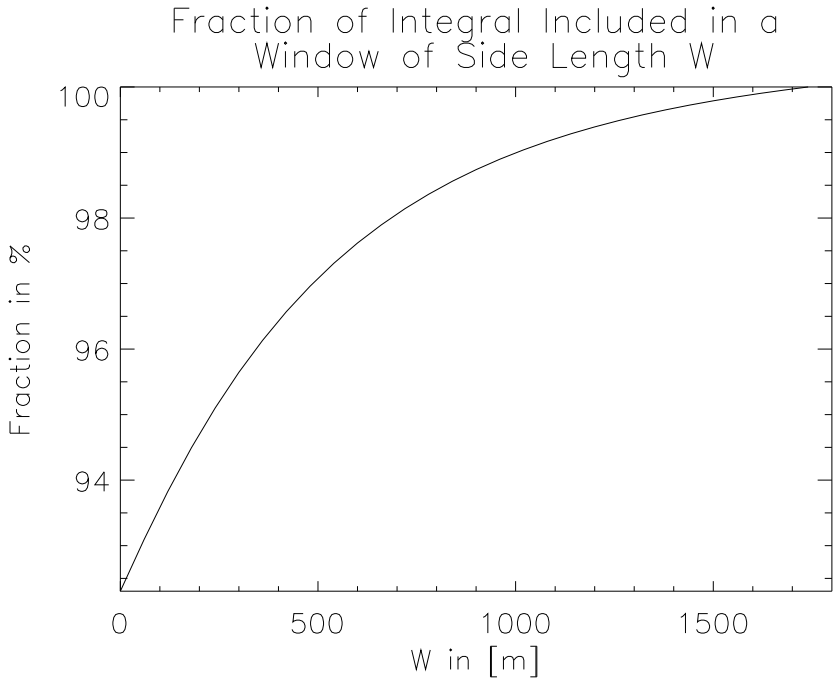

Figure 3 Normalized integral over the point spread function as a function of window size W in meters side length.

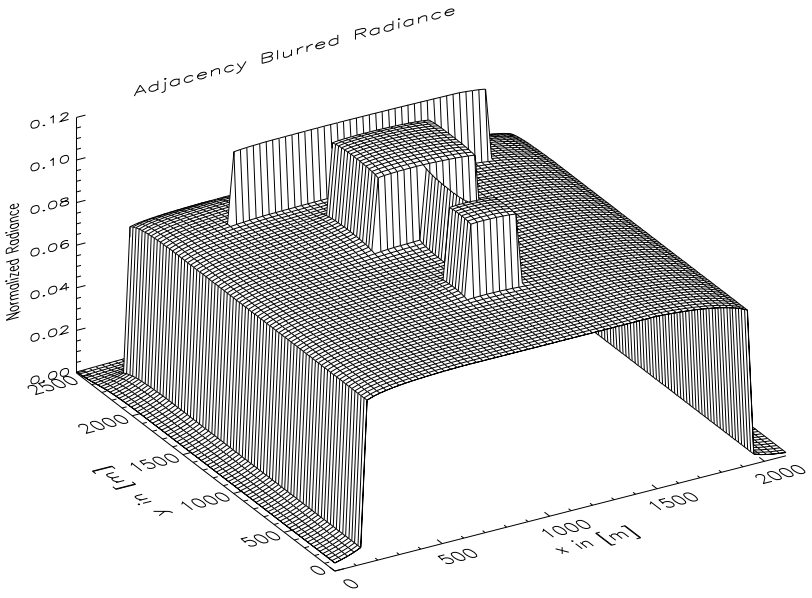

Figure 4 Normalized adjacency blurred radiance of a synthetic scene.

References

[1] C.C. Borel, S.A.W. Gerstl. "Simulation of partially obscured scenes using the radiosity method", *SPIE Vol. 1486*, pp.271-277, April 1991.

[2] D.J. Diner and J.V Martonchik. "Atmospheric transmittance from spacecraft using multiple view angle imagery", Applied Optics, 24:21, pp.3503-3511, 1985.

[3] H.C. Hottel and A.F. Sarofim. *Radiative Transfer.* McGraw-Hill Book Company, New York, New York, 1967.

[4] Y.J. Kaufman. "Atmospheric effects on remote sensing of surface reflectance", SPIE proceedings, 475:20-33, 1984.

[5] K.-N. Liou. *An Introduction to Atmospheric Radiation.* Academic Press, Orlando, FL, 1980.

[6] H.E. Rushmeier and K.E. Torrance. "The zonal method for calculating light intensities in the presence of a participating medium", *SIGGRAPH Proceedings*, 21(4):293, July 1987.

[7] W.A. Pearce. "A study of the effects of the atmosphere on thematic mapper observations", Report 004-77, EG&G, Washington Anal. Serv. Center, Riverdale, MD, 1977.

[8] W.K. Pratt. *Digital Image Processing.* John Wiley & Sons, New York, New York,1978.

[9] R. Richter. A fast atmospheric correction algorithm applied to Landsat TM images", Int. J. Remote Sensing, 11, pp.159-166, 1990.

[10] D. Tanré, M. Herman and P.Y. Deschamps. "Influence of the background contribution upon space measurements of ground reflectance", Applied Optics, 20:20, pp.3676-3684, 1981.